Agricultural and Forest Meteorology 329 (2023) 109267

Contents lists available at ScienceDirect

Agricultural and Forest Meteorology

journal homepage: www.elsevier.com/locate/agrformet

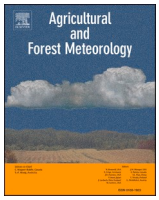

Carbon uptake by Douglas-fir is more sensitive to increased temperature and vapor pressure deficit than reduced rainfall in the western Cascade Mountains, Oregon, USA

Karla M. Jarecke [a,*], Linnia R. Hawkins [a], Kevin D. Bladon [b], Steven M. Wondzell [c]

[a] Department of Forest Ecosystems and Society, Oregon State University, Corvallis, OR 97331, USA
[b] Department of Forest Engineering, Resources, and Management, Oregon State University, Corvallis, OR 97331, USA
[c] USDA Forest Service, Pacific Northwest Research Station, Corvallis, OR 97331, USA

ARTICLE INFO

Keywords:
Gross primary productivity
Transpiration
Vapor pressure deficit
Douglas-fir
Soil-plant-atmosphere model

ABSTRACT

Understanding how trees respond to drought is critical to understanding forest sensitivity to global climate change, which can help inform forest policy and management decisions. However, mechanisms governing carbon fixation and water fluxes in response to increased temperatures and water limitation in regions with Mediterranean climates, with wet winters and dry summers, remain only partially understood. We tested the effect of increased vapor pressure deficit (VPD) and decreased rainfall on water and carbon fluxes of Douglas-fir (*Pseudotsuga menziesii*) trees using the Soil-Plant-Atmosphere model (SPA). We simulated a 50-year-old Douglas-fir stand on the western slopes of the Cascade Mountains in Oregon, USA. Simulation results showed that increasing the daily maximum VPD by 0.25–2.5 kPa during the summer increased cumulative transpiration by 1–3% and decreased cumulative gross primary production by 3–25%. In contrast, decreasing rainfall by 10–100% during the spring and summer decreased cumulative transpiration by 2–16% and decreased cumulative gross primary production by 0.5–4%. Transpiration was highly sensitive to decreases in rainfall, especially in late spring and early summer but much less sensitive to increases in maximum daily VPD. In contrast, gross primary productivity was much more sensitive to VPD, with summertime increases in VPD having a 5- to 6-fold greater effect on gross primary productivity than did decreasing the rainfall. These results suggested that temperature increases expected from climate change in combination with increases in VPD are likely to reduce forest productivity regardless of soil moisture availability.

1. Introduction

Climate change is projected to drive unprecedented increases in daytime vapor pressure deficit (VPD) in the Pacific Northwest, U.S.A. (Dalton et al., 2013; Rupp et al., 2017). The greatest increases in daily maximum VPD are expected to occur during the summer (June–August) when the region receives less than 10% of its annual rainfall (Daly et al., 2019). Increased VPD and low soil water availability during the summer can reduce plant carbon uptake (Littell et al., 2008; Novick et al., 2016; Restaino et al., 2016; Sulman et al., 2016). Thus, the combination of elevated VPD and reduced rainfall in the region is likely to exacerbate water stress in tree species without the physiological and structural strategies to cope with hotter droughts (Brodribb et al., 2020; Grossiord et al., 2017).

Tree physiological responses to large increases in temperature and VPD (e.g., heat waves) and decreased rainfall involve many interacting processes that encompass a wide range of species-specific strategies to deal with heat and drought stress (Liu et al., 2021; Venturas et al., 2017). When exposed to sunlight, it is advantageous for vascular plants to keep their stomata open so that carbon dioxide can diffuse into the leaf for photosynthesis (Lawson and Blatt, 2014). As temperature and VPD rise during the day, increased water loss via transpiration induces more tension on the water in the xylem, causing leaf water potential to drop (Meinzer et al., 2009; Phillips et al., 2002). As a result, some species will partially close stomata to limit xylem tensions that cause cavitation or leaf water potentials that drop below a critical minimum (Brodribb et al., 2020). In addition, low soil water content may also trigger plants to close their stomata earlier in the day to avoid dangerously low xylem

* Corresponding author.
E-mail address: karla.jarecke@oregonstate.edu (K.M. Jarecke).

https://doi.org/10.1016/j.agrformet.2022.109267
Received 6 April 2022; Received in revised form 15 November 2022; Accepted 29 November 2022

water potentials (Zweifel et al., 2007). Other studies have documented the combined effects of soil water availability (low plant-available soil water) and atmospheric drought (high VPD) on tree function; however, there is evidence that high VPD may have independent physiological effects on stomatal conductance without soil water limitations that require further investigation (Grossiord et al., 2020).

Disentangling the role of soil water availability and VPD on ecosystem water and carbon fluxes is difficult because they tend to be strongly correlated at monthly and seasonal time scales (Novick et al., 2016). Increased VPD from climate warming can reduce carbon uptake regardless of soil water status (Sulman et al., 2016) and high VPD can also increase rates of water loss from moist soils and set the stage for increased plant water stress due to more severe soil drought (Eamus et al., 2013). Vegetation sensitivity to drought stress may depend on subsurface water storage capacity relative to annual rainfall (Hahm et al., 2019) as well as the actual amount of plant-available water stored in the soil. For instance, plant-available soil water generally increases with increasing soil depth due to depth-dependent changes in soil physical characteristics that promote greater soil-water retention in deeper soils (Warren et al., 2005). This deep subsurface water storage (e.g., $>$ 1 m) can be a critical water source for trees in seasonally dry Mediterranean climates (Bales et al., 2018; Hahm et al., 2020). Thus, tree water stress caused by high VPD could be increasingly decoupled from soil drought (e.g., large daily increases in VPD with relatively small daily decreases in soil water) if subsurface water storage capacity and rooting depth is sufficient to sustain transpiration throughout the growing season. Still, our understanding of climate-driven impacts on forest ecosystems remains limited, in part, due to the uncertainty in how trees respond to increased temperature and VPD relative to decreased rainfall (Eamus et al., 2013; Grossiord et al., 2020).

In our study, we disentangled the relative effects of atmospheric demand and rainfall on carbon and water fluxes from 50-yr-old Douglas-fir (*Pseudotsuga menziesii*) trees growing on the western slope of the Cascade Mountains in Oregon, USA using the Soil-Plant-Atmosphere (SPA) model. Our specific objectives were to:

(a) determine how soil water availability, gross primary productivity, and transpiration respond to increased temperature and VPD (with no change in rainfall) during the summer;
(b) determine how soil water availability, transpiration, and gross primary productivity respond to decreased rainfall (with no change in temperature and VPD) during spring and summer;
(c) examine the interactive effects of increased VPD and decreased rainfall on gross primary productivity and transpiration.

2. Methods

2.1. Site description

We simulated gross primary production (GPP) and transpiration for 50-yr-old Douglas-fir (*Pseudotsuga menziesii*) trees growing in Watershed 1, a 96-ha catchment at the HJ Andrews Experimental Forest on the west slope of the central Cascade Mountains of Oregon, USA. The region experiences strong seasonality with cool, wet winters and warm, dry summers. The average elevation was 576 m and average slope was 37° at the sites where we collected soil data to parameterize the model. The overstory canopy is dominated by Douglas-fir trees with younger Western hemlock (*Tsuga heterophylla*) and Western red cedar (*Thuja plicata*) trees in the understory. Oregon grape (*Mahonia aquifolium*) and sword fern (*Polystichem munitum*) are the predominant understory shrub species. More information on the land management history can be found in Jarecke et al. (2021).

Soils in the study area are gravelly, silty clay loams. The organic horizon is approximately 5 cm thick and average depth to bedrock is 2.3 m (Jarecke et al., 2021). Hillslope soils are underlain by unconsolidated, highly weathered saprolite and fractured bedrock that allow for deep drainage so that saturation seldom occurs within the top 2 m of soil (Gabrielli et al., 2012; Jarecke et al., 2021). Tuffs and breccias are the most common parent materials, but basalts and andesites are also present (Halpern, 1988).

2.2. Model description

The Soil-Plant-Atmosphere model (SPA) was originally developed for a mixed deciduous forest to link stomatal behavior to plant hydraulic traits, canopy structure, soil properties, and atmospheric conditions (Williams et al., 1996). The SPA model simulates carbon and water fluxes at hourly time steps across a multi-layered tree canopy and soil profile. The model simulates transpiration using the Penman-Monteith equation (Monteith and Unsworth, 2008) and photosynthesis using the Farquhar model (Farquhar and von Caemmerer, 1982). Stomatal conductance is optimized to maximize carbon gain while avoiding hydraulic damage given species-specific hydraulic traits, including root-to-leaf conductance and a threshold for minimum leaf water potential. The hydraulic resistance of each canopy layer is assumed to increase with path length and is calculated from three parameters: stem hydraulic conductivity (mmol m^{-1} s^{-1} MPa^{-1}), canopy height (m), and leaf area of the canopy layer (m^2 m^{-2}) (Table 1). Photosynthetically active radiation, leaf temperature, leaf boundary layer conductance, and soil water supply are simulated for each canopy layer. The change in leaf water potential was determined iteratively at each time step using the simulated leaf-to-air VPD, transpiration rate, soil water potential, gravitational potential, and hydraulic resistance along the soil-to-leaf pathway. Greater leaf-to-air VPD, which is based on leaf temperature and the water deficit of the air, results in greater evapotranspiration rates for a given stomatal aperture. Thus, plants lose more water per unit carbon gain under higher atmospheric VPD with all else held equal. Additional details describing the SPA model can be found in Williams et al. (2001).

We used SPA version 3.0 with the modification used in Ruehr et al. (2014) to improve estimates of soil water retention. A sigmoid

Table 1
Parameters used in the Soil-Plant-Atmosphere model, which were derived from literature values or estimated using a Latin hypercube sampling scheme.

Parameters	Units	Source	Value
Foliar nitrogen concentration	g N m^{-2} leaf area	Berner and Law, 2016	1.08
Foliar carbon concentration	g C m^{-2} leaf area	Berner and Law, 2016	51.4
Leaf area index (LAI)	unitless	Barnard, 2009	7.5
Leaf capacitance	mmol m^{-2} MPa^{-1}	Licata, 2003	625
RuBP carboxylation catalytic rate coefficient at 30 °C (Vcmax)	μmol g^{-1} N s^{-1}	Licata, 2003	26.3
Electron transport rate coefficient at 30 °C (Jmax)	μmol g^{-1} N s^{-1}	Licata, 2003	74.73
Maximum rooting depth	m	Fan et al., 2017	2
Root resistivity	MPa s g $mmol^{-1}$	Bonan et al., 2014	25
Tree height	m	estimated	30
Soil porosity	m^3 m^{-3}	estimated	0.3
Whole plant (stem) hydraulic conductivity*	mmol m^{-1} s^{-1} MPa^{-1}	estimated	12
Water use efficiency*	unitless	estimated	537
Minimum leaf water potential*	MPa	estimated	−2.8
Total root biomass per volume*	g m^{-3}	estimated	1330
Root biomass to 50% of rooting depth*	g m^{-3}	estimated	150
Soil water retention constant a*	unitless	estimated	−0.015
Soil water retention constant b*	unitless	estimated	3.38
Soil water retention constant c*	unitless	estimated	0.159
Soil water retention constant d*	unitless	estimated	0.025

* Adjusted during model parameterization using a Latin hypercube sampling scheme.

relationship between soil water content and soil water potential was defined in place of the empirical relationships with soil texture from Saxton et al. (1986). We assigned values to model parameters that described tree attributes and physiology based on a typical 50-yr-old Douglas-fir tree in our study area (Table 1). We included four canopy layers at 21, 24, 27, and 30 m with equal leaf area in each layer. The vertical distribution and leaf area index of canopy layers affect the absorption of photosynthetically active radiation and other wavelengths of light. We used a 2 m soil profile divided into 20 layers, each 10 cm thick. The vertical profile of root biomass from the surface to the maximum rooting depth is represented in the model using an exponential decay function. The maximum rooting depth has been quantified as ~2 m for Douglas-fir (Mauer and Palátová, 2012; McMinn, 1963). Root distributions are highly variable and dependent on soil characteristics, topography, and plant physiology. This variability is challenging to represent in models. Thus, the rooting profile is likely an oversimplification but a reasonable approximation used by many Earth system models. Soil properties, including soil porosity and soil water retention, were held constant throughout the soil profile and were determined from field observations and model parameterization. We used model outputs of leaf water potential for the top canopy layer and weighted soil water potential ($SWP_{weighted}$) to evaluate tree water stress. Weighted soil water potential adjusts to the maximum potential water uptake in each soil layer (E_l), defined as the difference between soil water potential for each soil layer (SWP_l) and the minimum leaf water potential (LWP_{min}) divided by the hydraulic resistance of soil and roots in each soil layer (R_l):

$$E_l = \frac{SWP_l - LWP_{min}}{R_l}$$

The estimate of E_l was then used to determine the $SWP_{weighted}$ for the rooting zone:

$$SWP_{weighted} = \frac{\sum_{i=l}^{l}(SWP_i\ E_i)}{\sum_{i=l}^{l}(E_i)}$$

2.3. Model parameterization and meteorological drivers

The SPA model parameters for Douglas-fir were determined from the literature wherever possible. We used a spin-up period of 15 months—from January 2018 to March 2019—to establish initial conditions before the period of model calibration, from March to September 2019. We used meteorological data from the HJ Andrews Experimental Forest for model spin-up and calibration (Fig. 1). Rainfall, temperature, relative humidity, wind speed, and shortwave radiation were recorded every 15 min at the Primary Meteorological Station (PRIMET) and aggregated to hourly data using the mean for all variables except rainfall, which was summed. We calculated VPD from air temperature and relative humidity. Photosynthetically active radiation was calculated as 50% of shortwave radiation, which was measured 1 m above the ground in a

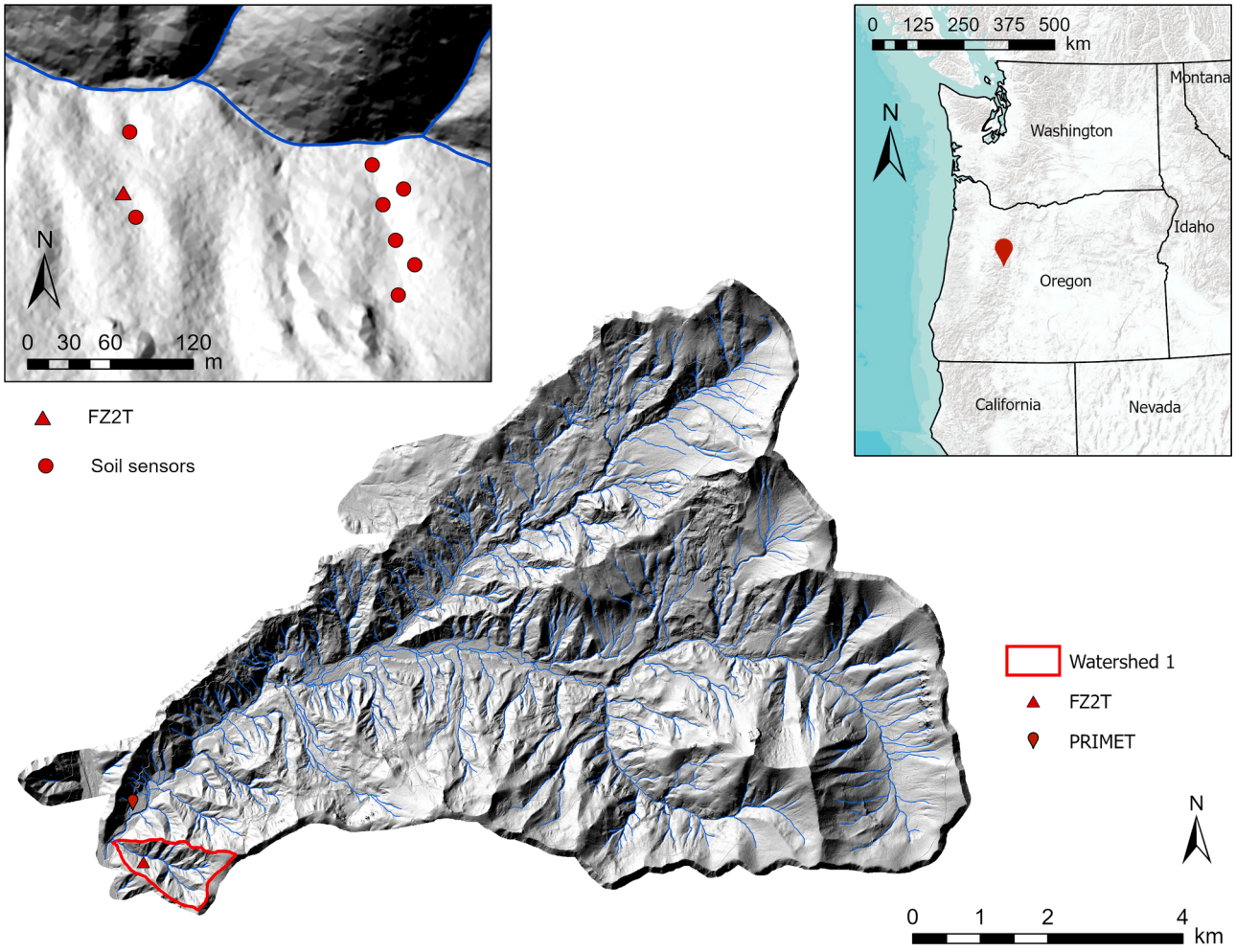

Fig. 1. Location of Watershed 1 at the HJ Andrews Experimental Forest near Blue River, Oregon. Soil water content at 50 cm was collected along two hillslopes at nine sites. Soil water content at site FZ2T (red triangle) was used to calibrate the Soil-Plant-Atmosphere model. Meteorological drivers including rainfall, air temperature, relative humidity, wind speed, and shortwave radiation were collected at the Primary Meteorological Station (PRIMET) located at the HJ Andrews headquarters.

clearing at PRIMET. The CO_2 concentration was obtained from the US-Me2 AmeriFlux tower (Law, 2021) located in central Oregon, approximately 55 km northeast of PRIMET. The Primary Meteorological Station received 1948 mm of rainfall during the 2019 water year. The average annual rainfall for water years 1989–2019 was 2212 ± 427 mm. Thus, annual rainfall for the 2019 water year was 263 mm below the long-term average, but this difference was well within the standard deviation. The maximum annual rainfall from 1980 to 2019 was 3244 mm, and the minimum was 1276 mm.

Soil moisture calibration data were collected at nine sites along two north-facing hillslopes (Fig. 1) with similar slope and tree density (Jarecke et al., 2021). Soil moisture and water potential sensors (5TM and TEROS 21, METER Environment) were installed horizontally into undisturbed soil at 50 cm depth in October 2018 to record hourly data. We calculated volumetric soil water content (SWC) from the dielectric permittivity using the manufacturer's equation, which follows Topp et al. (1980). The measurement error for soil water content using the default calibration setting of the sensor was 0.03 m^3 m^{-3}. We evaluated the mean daily SWC calculated for each site and calibrated the model using data from the single site that best represented the median daily SWC across all sites from March to September 2019 (Fig. 2a).

Model parameters were adjusted iteratively to produce the best agreement between simulated and observed SWC at 50 cm depth (Fig. 2a). This process was performed with nine parameters—stem conductance, water use efficiency, minimum leaf water potential, total root biomass, root biomass to 50% of rooting depth, and four constants that define the shape of the soil water retention curve (Table 1). We used a Latin hypercube sampling scheme (McKay et al., 2000) to generate combinations of parameter values within a predefined range for each parameter with a sample size of $n = 100$ parameter sets. The ranges for soil water retention parameters were based on our estimates of soil water retention from field observations of SWC and soil water potential at 50 cm during a period without rainfall from July 1–August 10, 2019. All other ranges were based on literature values from studies of conifer forests or were estimated when no literature values were found (Table 1). Model simulations were ranked according to their agreement with observed daily SWC at 50 cm between March and September 2019. We selected the model parameterization that was within the top five models based on lowest RMSE and highest R^2 between simulated and observed values. Next, we ran the model with meteorological data from

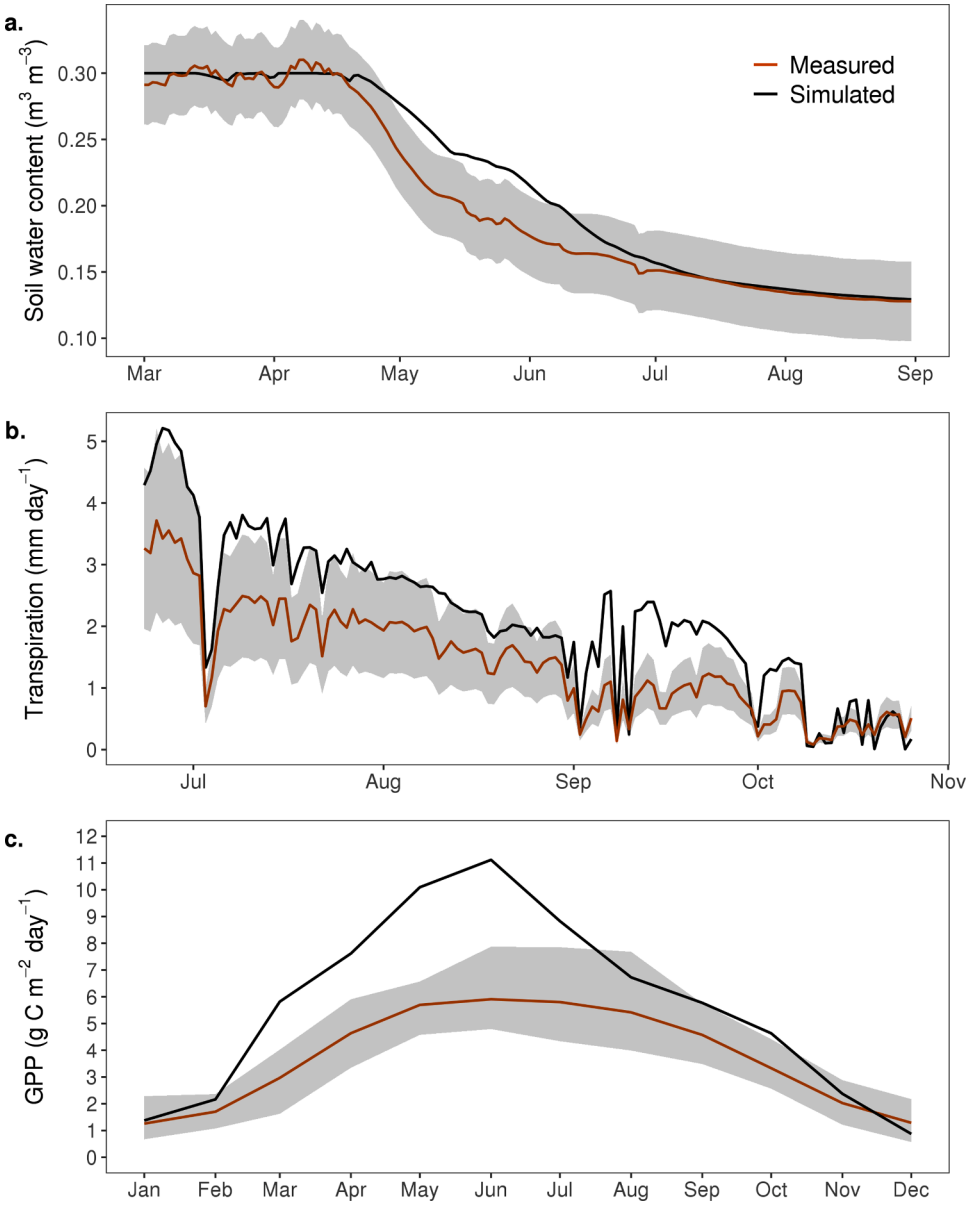

Fig. 2. Mean daily soil water content at 50 cm between March and September 2019 (a) and daily transpiration between June and October 2000 (b) were measured in Watershed 1 at the HJ Andrews Experimental Forest. Mean monthly GPP was measured at the Wind River Experimental Forest eddy covariance tower from 1999 to 2015 and compared to the simulated mean monthly GPP from the 2019 baseline model for Watershed 1 (c). Error estimates for observational data (gray shading) are based on the measurement accuracy of sap flow and soil water content and the 5th and 95th percentiles of the mean monthly GPP.

January 1999 to October 2000 and checked the match between simulated and empirical transpiration, which was measured in ~30-year-old Douglas-fir between June and October 2000 (Moore et al., 2004; Moore and Bond, 2007) (Fig. 2b). Measurements of sap flow are known to have substantial error—as such, we applied $a \pm 40\%$ error band around the empirical transpiration data prior to comparisons with the simulated data (Ruehr et al., 2014). The model estimates of mean monthly GPP were also checked for agreement with estimates of mean monthly GPP from eddy covariance measurements in an old-growth Douglas-fir/western hemlock stand in the Wind River Experimental Forest in south-western Washington. All model simulations were performed using the calibrated parameterization, and no offset was applied.

2.4. Climate scenarios

Climate scenarios were defined relative to baseline meteorological input from March to August 2019—hereafter referred to as the "baseline scenario". First, we tested the effect of increased VPD between June and August 2019 (hereafter referred to as "summer") on GPP and transpiration fluxes from Douglas-fir. Second, we tested the effect of decreased rainfall between March and August 2019 (hereafter referred to as "spring and summer") to simulate soil drought conditions during the growing season. We compared model output under the modified climate scenarios to the baseline scenario to evaluate the effects of increased VPD and decreased rainfall on GPP and transpiration. We changed VPD and temperature while keeping rainfall at baseline conditions. Then we changed rainfall while keeping VPD and temperature at baseline conditions. Lastly, we examined the interactive effects of increased VPD and decreased rainfall on GPP and transpiration by increasing VPD across the different levels of decreased rainfall and vice versa.

We established climate scenarios to test the independent effect of each factor—increased VPD and decreased rainfall—with the objective of modeling a range of conditions from mild to severe atmospheric and soil drought. We used the long-term climate record from PRIMET (Daly et al., 2019) to determine average conditions of maximum daily VPD and temperature during the summer. The daily maximum VPD during the summer from 1989 to 2019 averaged 2.4 ± 1.3 kPa and the daily maximum temperature averaged 26.7 ± 6.1 °C. We developed 10 VPD scenarios of varying severity in which we increased the VPD in increments of 0.25 kPa from +0.25 to +2.5 kPa. We refer to these scenarios as 'vpd0.25', 'vpd0.5', and so on. The most extreme warming scenario, vpd2.5, is approximately two standard deviations above the long-term average. We increased the hourly VPD in 2019 ($VPD_{baseline}$) as a proportion of the daily max VPD ($VPD_{baseline\ daily\ max}$).

$$VPD_{new} = VPD_{baseline} + increase\ in\ daily \max VPD\left(\frac{VPD_{baseline}}{VPD_{baseline\ daily\ max}}\right)$$

This allowed for a minimal increase in VPD during nighttime hours and maximum increase in VPD as it approached the daily maximum (Fig. 3a). After determining the VPD time series, we calculated the increase in air temperature necessary to achieve the desired hourly VPD without changing the actual vapor pressure. The result was an increase in hourly air temperature with the maximum increase in temperature occurring mid-day when VPD was greatest (Fig. 3b).

Similarly, we developed 10 rainfall scenarios by decreasing the 2019 hourly rainfall by 10% increments from 100% (no change in rainfall) to 0% (no rainfall) between March and August. The baseline scenario, referred to as 'rain100', received 726 mm of rain between March and August. Removal of all rainfall between March and August was called 'rain0'. For comparison, the total rainfall between March and August from 1989 to 2019 averaged 762 ± 184 mm. Total rainfall in the rain50 scenario is approximately two standard deviations below the long-term average whereas no rainfall in the rain0 scenario is four standard deviations below the long-term average.

We evaluated the independent effect of increased VPD and decreased rainfall by calculating the difference in cumulative summer GPP and transpiration between the baseline scenario and each of the climate scenarios. Negative values for change in cumulative GPP and

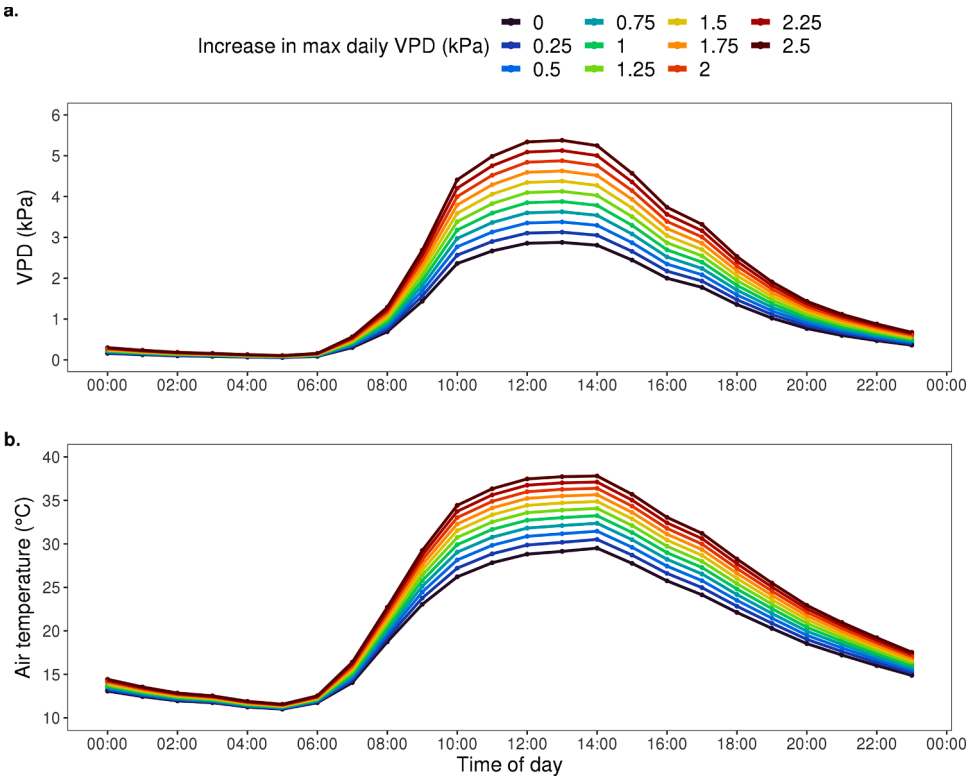

Fig. 3. Hourly vapor pressure deficit (VPD, a) and hourly air temperature (b) on July 14 under the ten climate scenarios that increased the daily maximum VPD, relative to 2019 conditions.

transpiration indicate a reduction with respect to the baseline scenario. We also evaluated the interactive effect of increased VPD and decreased rainfall on cumulative GPP and transpiration by running each VPD scenario ($n = 10$) at each level of decreased spring and summer rainfall ($n = 10$). We created a catalog of input files using R version 4.1.0 (R Core Team, 2021). We looped through the input files placing them in the default directory for SPA and ran the model by submitting a text string to the command line using the system() function. All data analysis and processing were performed in R version 4.1.0 (R Core Team, 2021) and using the dplyr (Wickham et al., 2021), tidyr (Wickham, 2021), cowplot (Wilke, 2020), and ggplot2 (Wickham, 2016) packages.

3. Results

3.1. Model agreement with observations

The simulated baseline transpiration from the calibrated Soil-Plant-Atmosphere (SPA) model agreed with field measurements reported by Moore et al. (2004) in the same watershed (Fig. 2b). Their estimates of transpiration rates from June to October of 2000 ranged from 0.1 to 3.7 mm day^{-1}, whereas the simulated baseline transpiration rates ranged from 0.1 to 5.2 mm day^{-1}. The peak transpiration in late June in our baseline scenario was nearly 40% greater than measured transpiration reported by Moore et al. (2004) during this period. The discrepancy between the maximum simulated transpiration and the observed maximum could have resulted from either overestimating shallow root density in the model or with potentially large errors associated with scaling sap flow measurements (Moore et al., 2020). While simulated and observed transpiration values did not always agree in magnitude, transpiration in our baseline simulation adequately reflected day-to-day variability and seasonal trends. Cool spring temperatures limited transpiration when water was plentiful (i.e., atmospheric demand was less than potential rates of supply). In contrast, an increase in evaporative demand in late spring resulted in increased transpiration rates; however, transpiration declined by late summer when water stress increased.

Our simulation of gross primary productivity (GPP) between June and August (6 to 11 g C m^{-2} day^{-1}) was greater than observations reported for a similar forest type and climate at Wind River Experimental Forest in southwest Washington, USA where estimated GPP ranged from 4 to 5 g C m^{-2} day^{-1} between June and August (Fig. 2c). While the simulated peak GPP in our study was considerably greater than the observed GPP at Wind River, the seasonal dynamics of GPP in our baseline simulation agreed with the seasonal dynamics observed at Wind River. In our study, GPP increased from March to June as temperatures and photosynthetically active radiation increased and declined during July and August with increased evaporative demand and soil water stress. Although the magnitude of simulated spring GPP at our site was higher than observed at Wind River, the two forests were not directly comparable given the considerable differences in age, stand density, and leaf area index. Furthermore, the species composition at Wind River was notably different from the HJ Andrews Experimental Forest. The forest at Wind River was composed of nearly 40% western hemlock, a shade tolerant species with lower photosynthetic rates than Douglas-fir (Winner et al., 2004), which dominate the HJ Andrews Experimental Forest. We acknowledge that the modeled transpiration and GPP rates are at or above the estimated range from observations; however, given that our study was designed to examine relative changes in transpiration and GPP— not absolute magnitudes—we considered the model performance to be adequate.

3.2. Effects of increased VPD and decreased rainfall on soil water

We found that reducing rainfall during the winter (from January to March) had no effect on simulated soil water storage due to the lack of evaporation and transpiration during this time (results not shown). Thus, the simulated soil water content was at saturation, or 0.3 m^3 m^{-3}, at the beginning of our scenarios in March. Total rainfall in the baseline scenario was 121 mm in March 2019 and 374 in April 2019. This was lower than the long-term average rainfall of 254 mm in March and greater than the long-term average of 207 mm in April (Fig. 4a, Table 2). Decreasing rainfall during March and April had very little effect on the average soil water content and soil water potential except for the scenario that removed all rainfall (rain0), which caused soil water content in late April to decline from the baseline scenario by 0.04 m^3 m^{-3} at 20 cm and 0.02 m^3 m^{-3} at 50 cm (Fig. 5a).

Although the monthly means for daily maximum VPD in the vpd2.5 scenario increased by more than 2 kPa from the long-term monthly means (Fig. 4b, Table 3), shallow soil water content was more strongly influenced by decreased rainfall in May and June than by increased VPD from June through August. Simulated soil water content at 20 cm returned to saturation in late May in all scenarios where the precipitation inputs were 60% to 100% of the baseline rainfall during May and June. However, soil water content did not increase substantially in any scenario with less than 60% rainfall (Fig. 5a, c). For the low rainfall scenarios, the relatively low water content of the shallow soil layers in July triggered greater rates of soil water uptake at 100 cm. For example, soil water content at 100 cm was 0.04 m^3 m^{-3} lower in rain0 than in rain100 by the end of August (Fig. 5a, c). We also observed a decrease in soil water content at 20, 50, and 100 cm due to increased VPD during the summer. However, the changes in soil water content and soil water potential were relatively small, especially for deeper soil layers (Fig. 5b, d). Notably, scenarios of increased VPD eventually created a decline in soil water content and soil water potential at 100 cm by August when shallow soil water became more limiting and root water uptake from deeper soil layers increased.

3.3. Temporal dynamics of ecosystem stress with decreased rainfall

The effect of rainfall on water and carbon fluxes were dynamic over time. The daily maximum leaf water potential (hereafter referred to as leaf water potential) and root density weighted soil water potential (hereafter referred to as soil water potential) were relatively unaltered by the amount of rainfall in March and April (Fig. 6a). Thus, it was not surprising that GPP and transpiration were similar among rainfall scenarios during this time. In contrast, difference in the rainfall amounts in May and June created noticeable differences in leaf- and soil-water status. The rainy period in May created large differences in leaf and soil water potential that persisted through mid-June (Fig. 6a). Reduced rainfall led to lower leaf and soil water potentials during this period and, as a result, rates of GPP and transpiration decreased relative to the baseline scenario.

We observed a convergence in leaf and soil water potential among rainfall scenarios in June (Fig. 6a, arrow 1). However, a rain event in late June led to a temporary increase in leaf and soil water potential and increased transpiration and GPP in scenarios receiving 50% or more of the baseline rainfall (Fig. 6a). The higher rates of transpiration depleted the additional soil water and ultimately reduced soil water potential for the rain50–rain100 scenarios by late July. In contrast, the rain events in late June did not sufficiently increase soil water availability in scenarios receiving less than 50% of the rainfall. This caused transpiration to decline consistently, reducing the degree of soil water loss by late July relative to scenarios receiving more than 50% of the rainfall. The feedbacks between transpiration and soil water eventually created lower soil water potential in the baseline scenario (rain100) than the most extreme drought scenario (rain0) by late July (Fig. 6a, arrow 2). Following the dry period, a small rain event in late August created a temporary increase in leaf water potential, soil water potential, GPP, and transpiration for scenarios with $>$ 70% rainfall.

3.4. Temporal dynamics of ecosystem stress with increased VPD

In general, increasing the maximum daily VPD by 0.25–2.5 kPa

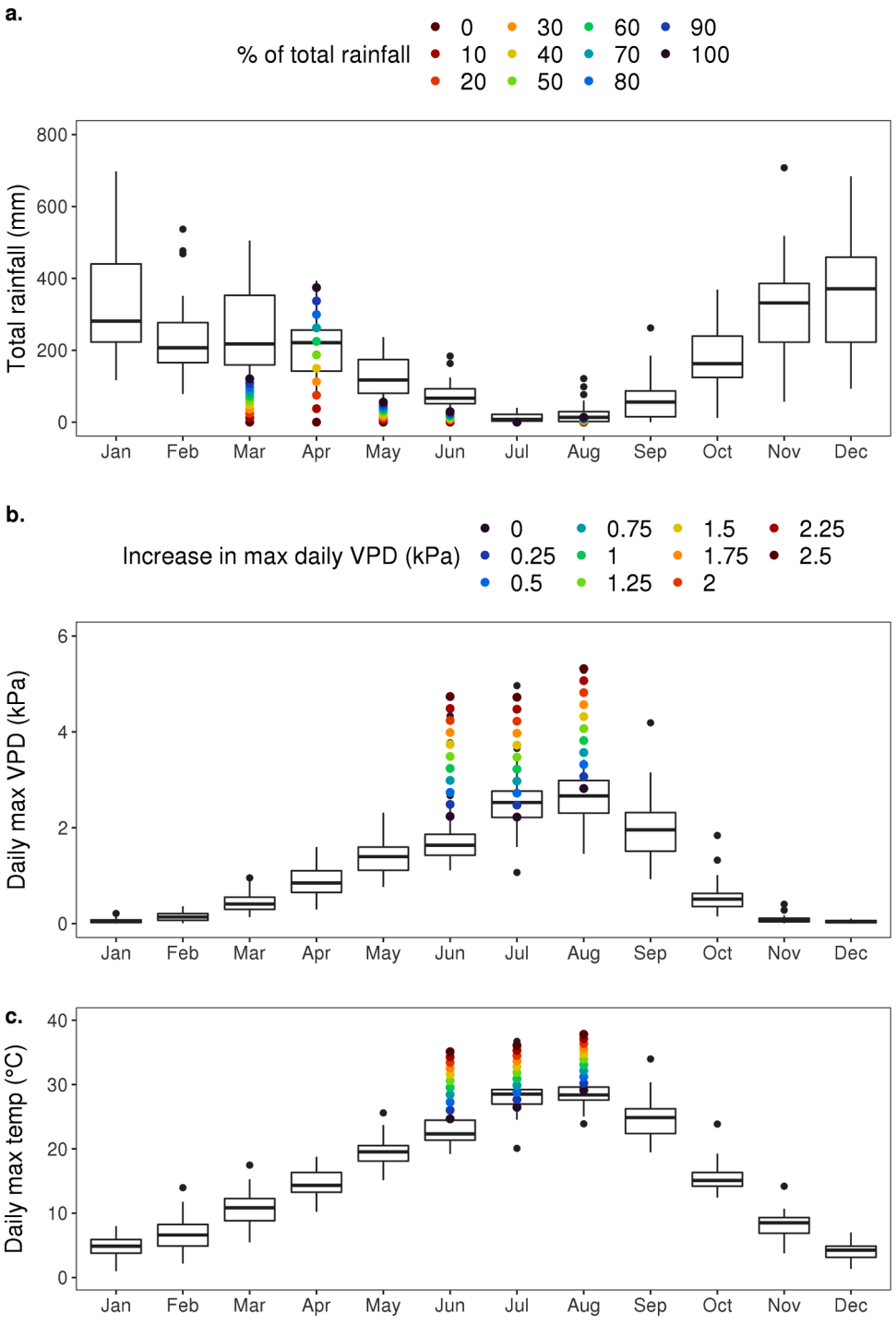

Fig. 4. Distribution of monthly total rainfall (a), monthly mean daily maximum vapor pressure deficit (VPD, b), and monthly mean daily maximum air temperature (c) from 1989 to 2019 and monthly means for experimental climate scenarios that increase daily max VPD during June, July, and August and decrease rainfall from March to August. The boxplot shows the interquartile range which included the median, 25th, and 75th percentiles with whiskers representing the smallest and largest values no further than 1.5 times the interquartile range. Extreme outliers beyond the whiskers were omitted from the graphic to improve visualization of data.

Table 2
Minimum, maximum, and mean monthly rainfall from 1989 to 2019 compared to 2019 conditions (rain100).

	mean	min	max	rain100 (2019)
March	254	41	505	121 mm
April	207	87	239	374 mm
May	127	9	236	56 mm
June	73	8	184	29 mm
July	13	0	40	0.3 mm
August	23	0.3	121	13 mm

(vpd0.25–vpd2.5) during the summer increased transpiration, which reduced soil water potential relative to the baseline scenario (vpd0) (Fig. 6b). However, we also observed a decrease in transpiration during periods when leaf and soil water potential fell below −1.0 MPa. Periods of relatively low leaf and soil water potential occurred from mid-June to mid-July. The greatest decrease in transpiration relative to the baseline scenario occurred in July when leaf and soil water potential were lowest (Fig. 6b, arrow 3). Conversely, we found that increased transpiration under periods of relatively lower water stress prompted a lagged effect on leaf and soil water potential by late July such that leaf and soil water potential converged among all VPD scenarios (e.g., Fig. 6b, arrow 4). The convergence of leaf water potential among scenarios led to an

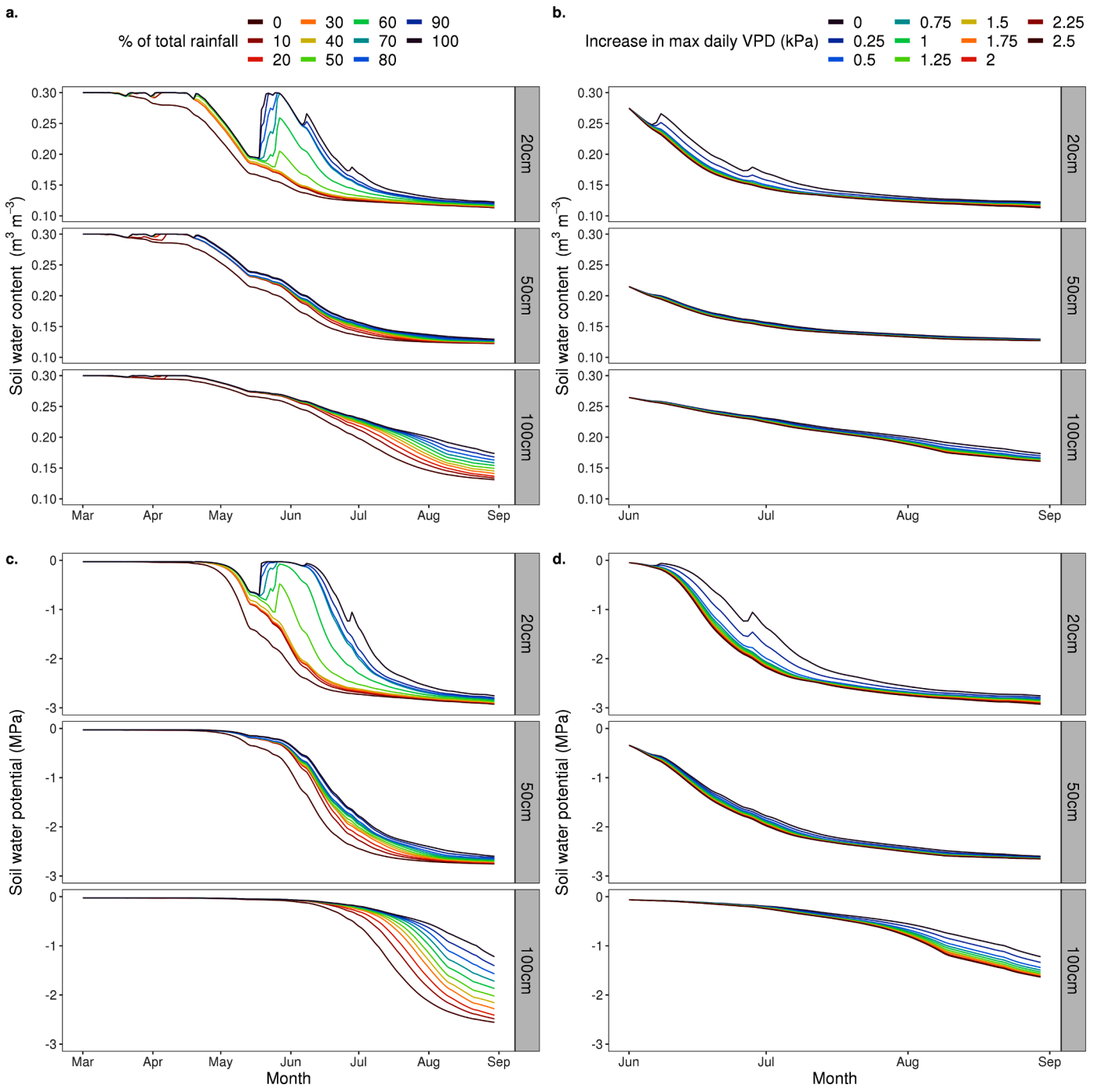

Fig. 5. Simulated soil water content and soil water potential at 20, 50, and 100 cm for decreased rainfall from March to August (a, c) and increased vapor pressure deficit (VPD) from June to August (b, d).

Table 3
Minimum, maximum, and mean daily max vapor pressure deficit (VPD) and air temperature from 1989 to 2019 compared to mean daily max VPD and mean daily max temperature in 2019 (vpd0).

	mean	min	max	vpd0 (2019) mean	vpd2.5 mean
June	1.82 kPa	1.11 kPa	4.33 kPa	2.2 kPa	4.7 kPa
	23.2 °C	19.2 °C	34.1 °C	24.7 °C	35.1 °C
July	2.55 kPa	1.07 kPa	4.96 kPa	2.2 kPa	4.7 kPa
	28.3 °C	20.1 °C	36.7 °C	26.5 °C	36.1 °C
August	2.69 kPa	1.46 kPa	5.29 kPa	2.8 kPa	5.3 kPa
	28.5 °C	23.9 °C	37.3 °C	29.1 °C	37.8 °C

increase in transpiration for scenarios of elevated VPD.

The effect of increased VPD on GPP persisted throughout the summer. We observed a decrease in GPP as the daily max VPD increased from 0.25 to 2.5 kPa (Fig. 6b). The greatest percent decreases in GPP from the baseline scenario (vpd0) to the most extreme increase in VPD (vpd2.5) occurred in late August when leaf water potential showed a sharp decline. The smallest difference in GPP among VPD scenarios occurred when leaf and soil water potential were similar across scenarios (e.g., Fig. 6b, arrow 4).

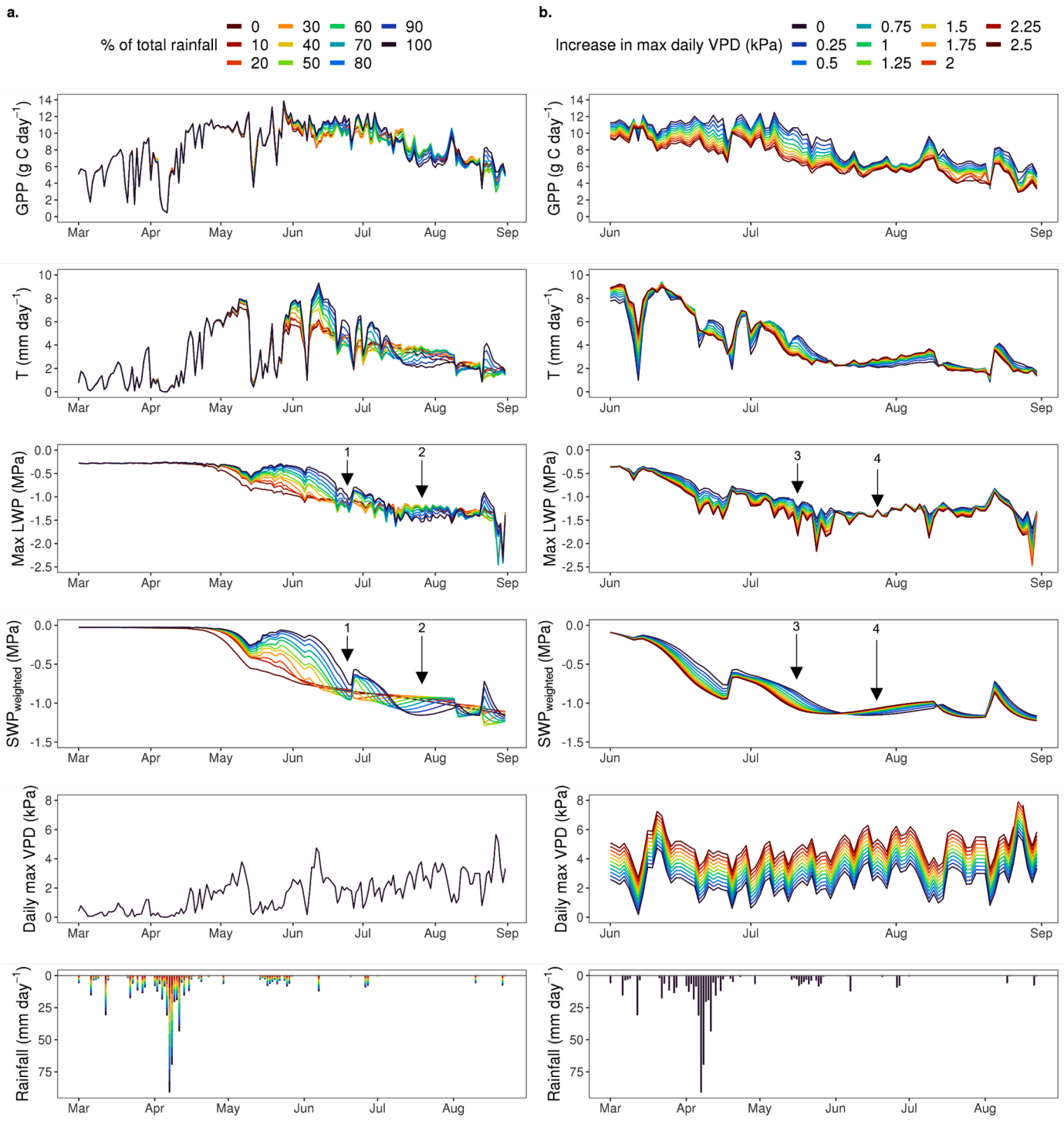

Fig. 6. Model results for daily total transpiration (T), daily total gross primary production (GPP), daily max leaf water potential (LWP), and weighted soil water potential ($SWP_{weighted}$) under various scenario for rainfall (a) and daily max vapor pressure deficit (VPD, b). The baseline model conditions for daily max VPD and rainfall in 2019 are shown. Experimental changes to rainfall occurred from March 1–August 31 and experimental changes to VPD and air temperature occurred during the climatological summer, June 1–August 31.

3.5. Effect of VPD and rainfall scenarios on cumulative GPP and transpiration

Increased VPD had a greater effect on cumulative GPP than did decreased rainfall. Scenarios in which maximum daily VPD increased by 0.25–2.5 kPa caused cumulative GPP over the summer to decrease by 23–200 g C or 3–25% (Fig. 7b). In contrast, as scenarios received less and less rainfall (i.e., rain90 through rain0), the GPP accumulated over the summer decreased from 4 to 33 g C or 0.5–4% (Fig. 7a). Increasing daily max VPD by 0.25 kPa and decreasing rainfall by 40% both led to a similar reduction in GPP. The differential sensitivity to VPD versus rainfall was surprising. For example, eliminating all rainfall from March through June only decreased cumulative GPP by 33 g C whereas, a 0.5 kPa increase in daily max VPD from June through August decreased cumulative GPP by 44 g C (Fig. 7).

Scenarios that reduced rainfall from 10 to 100% with no change in

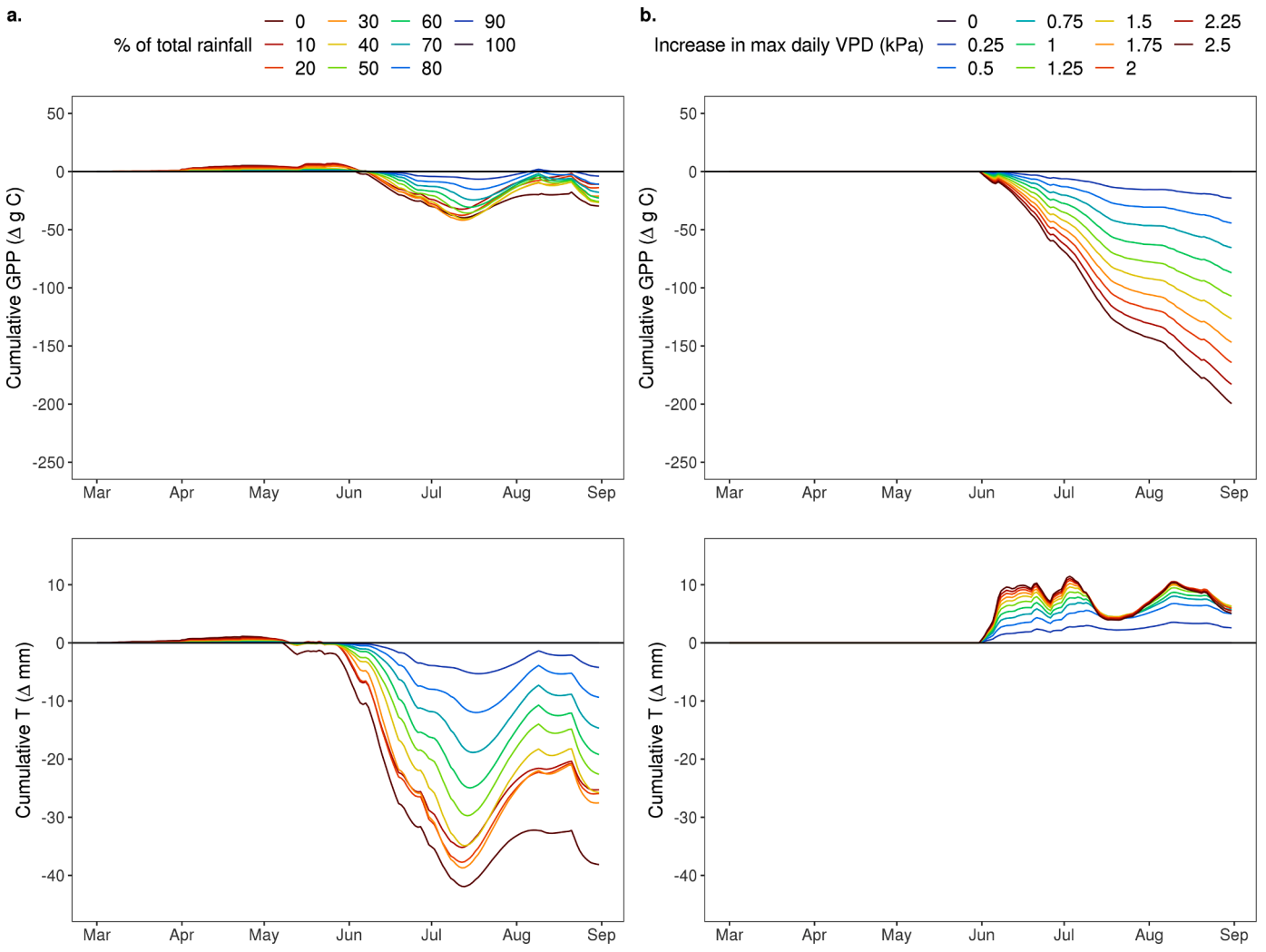

Fig. 7. The difference in cumulative gross primary productivity (GPP) and transpiration (T) from the 2019 baseline model (Δ = 0) in response to decreased rainfall scenarios from March to August (a) and increased vapor pressure deficit (VPD) scenarios from June to August (b).

VPD had a greater effect on cumulative transpiration from June 1 to August 31 than those that increased max daily VPD by 0.25–2.5 kPa with no change in rainfall. Cumulative transpiration over the summer decreased from the baseline scenario by 4–33 mm or ~2–16% due to reduced rainfall (Fig. 7a). In contrast, cumulative transpiration increased by only 3–6 mm or ~1–3% due to increased VPD (Fig. 7b).

The differences in cumulative GPP and transpiration among model scenarios varied throughout the growing season (Fig. 7). Cumulative GPP decreased monotonically from the baseline over time for scenarios with increased VPD while cumulative transpiration diverged from the baseline during June, began to converge in mid-July, and diverged again from late-July to mid-August (Fig. 7b). In contrast, cumulative GPP and transpiration decreased from the baseline scenario in response to decreased rainfall. The greatest divergence from the baseline occurred in mid-July, after which cumulative GPP and transpiration began to converge towards the baseline (Fig. 7a).

Simulations in which we changed both rainfall and VPD indicated that GPP was very sensitive to change in VPD (Fig. 8a), whereas transpiration was more sensitive to change in rainfall (Fig. 8d). There was clearly an interactive effect because cumulative GPP was lower with less rainfall (Fig. 8b), but this effect was small relative to the change in cumulative GPP across the range of VPD scenarios (Fig. 8a). Similarly, there was an interactive effect of decreased rainfall and increased VPD on cumulative transpiration. Cumulative transpiration was greater with elevated VPD (Fig. 8c), but this effect was small relative the change in cumulative transpiration across the range of rainfall scenarios (Fig. 8d). Additionally, VPD appeared to have more of an effect on cumulative transpiration for scenarios with 0–50% of total rainfall than scenarios with more than 60% of total rainfall (Fig. 8d).

4. Discussion

4.1. Effects of increased VPD vs. decreased rainfall on GPP and transpiration

The results of our modeling study suggested that climate-driven reductions in forest productivity on the west slope of the central Cascade Mountains of Oregon, USA are more likely to result from increases in VPD than from decreases in rainfall. Specifically, we observed greater declines in cumulative gross primary productivity (GPP) of Douglas-fir associated with modeling scenarios where we increased VPD relative to scenarios where we reduced rainfall inputs. The projected temperature increases from 2014 to 2070 in the Northwest U.S. range from 1.2 to 4.7 °C under the Representative Concentration Pathway 4.5 (Mote et al., 2013). At the lower end of this range, our climate scenario simulated an average increase in maximum daily temperature of 1.2 °C between June 1 and August 31, which was associated with an increase in maximum daily VPD of 0.25 kPa. This scenario (vpd0.25) caused cumulative GPP to decline by 3% of total GPP during the summer (June 1 to August 31). Comparatively, an increase in maximum daily temperature by 5 °C

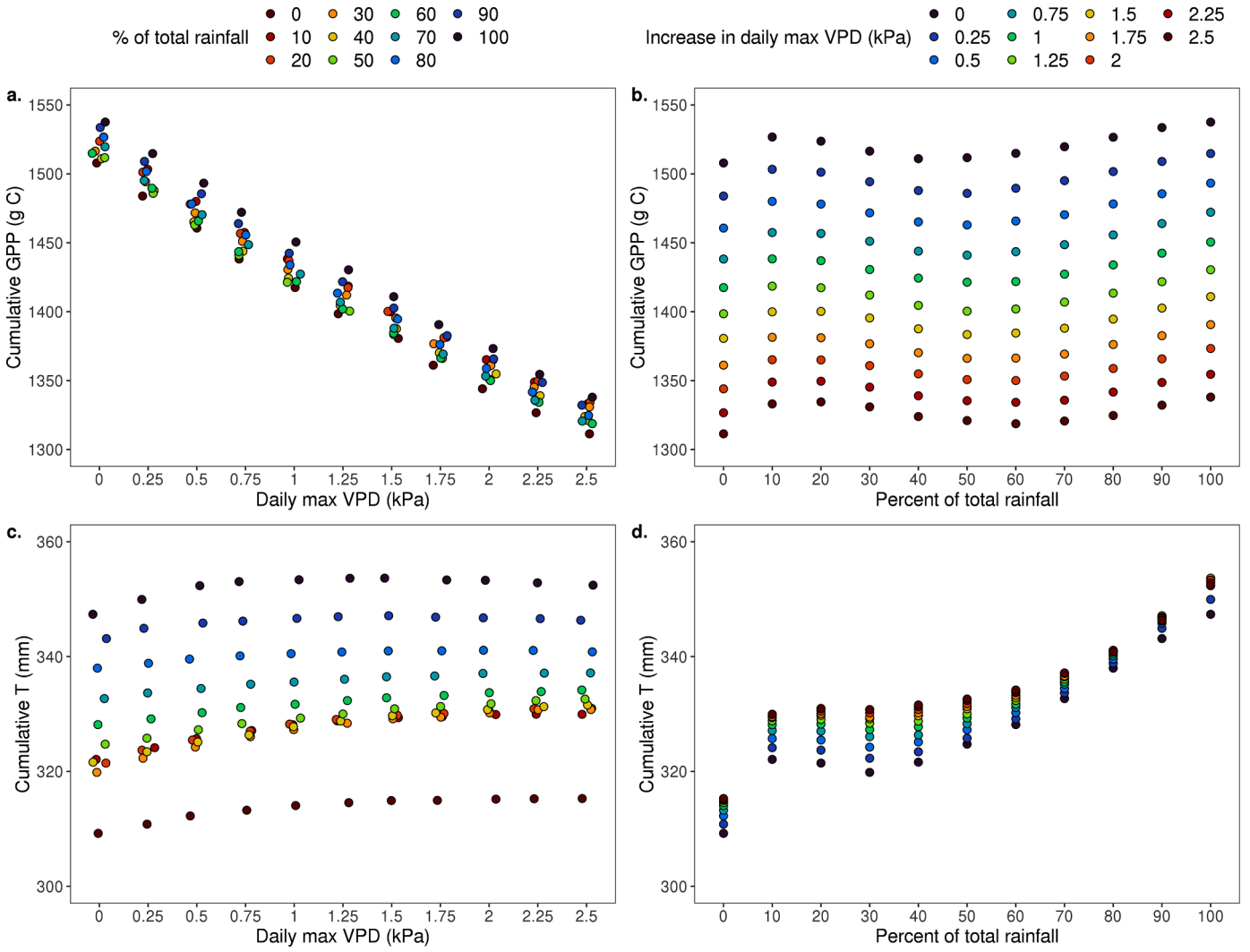

Fig. 8. The interactive effect of decreased rainfall and increased vapor pressure deficit (VPD) on cumulative gross primary production (GPP) and cumulative transpiration (T) from March–August with colors representing percent of total rainfall (a, c) and increase in daily max VPD (b, d).

during the summer was associated with an increase in maximum daily VPD of 1.0 kPa. This scenario (vpd1.0) caused cumulative GPP to decline by 11%. This decline in GPP in the vpd1.0 scenario was much greater than the decline in GPP after removing all spring and summer rainfall, which only resulted in a 4% decline in summer GPP. This extreme rainfall scenario is at the upper end of the range of our climate scenarios for decreased precipitation. The more likely scenario for the Pacific Northwest, with a 30% reduction in summer precipitation (Mote et al., 2013), simulated a cumulative GPP decline of only 2% (Fig. 7a).

The stronger response of GPP to atmospheric drought (i.e., increased air temperature and VPD) was consistent with decreases in stomatal aperture to prevent hydraulic failure. Douglas-fir have isohydric water use strategies, which allows them to conserve water while maintaining a relatively constant midday leaf water potential (Bond and Kavanagh, 1999). Thus, when VPD is high during the summer, Douglas-fir tend to reduce their stomatal opening earlier in the day to prevent xylem cavitation and embolism, which is consistent with the strong decline in carbon assimilation with increased temperature and VPD in our simulations. However, high temperatures can directly reduce rates of photosynthesis (Marias et al., 2017).

The direct effect of temperature on photosynthesis could confound our model results because our scenarios were developed by holding relative humidity constant and increasing air temperature to increase VPD. Our scenarios were thus consistent with global change projections which commonly report expected changes in temperature and precipitation but not relative humidity. Therefore, we examined the direct effect of temperature on photosynthesis by simulating an increase in temperature with a corresponding increase in relative humidity so that VPD would remain constant. Our results showed a 10% decline in cumulative GPP with a 9.5 °C increase in summer air temperature but showed a 25% decline in cumulative GPP with the corresponding vpd2.5 scenario. These results are dependent on the summer temperatures and aridity in the baseline model as well as the temperature optimum for individual species and thus will vary among ecosystems and across species with different temperature response curves. Nevertheless, these results suggested that the simulated declines in GPP in our scenarios were associated with both increased temperature and increased atmospheric drought. The decline in carbon assimilation due to heat-driven increases in VPD is also supported by other studies, which have observed a direct impact of VPD on canopy conductance without soil water limitation (Eamus et al., 2013; Fu et al., 2022; Grossiord et al., 2017; Novick et al., 2016; Ruehr et al., 2014; Sulman et al., 2016). For example, Ruehr et al. (2014) simulated high temperature and VPD under irrigated conditions in a semi-arid pine forest in eastern Oregon and found GPP continued to decline due to high VPD after soil water stress was removed. Moreover, they found greater declines in GPP associated with elevated summer air temperatures and VPD (−17%) compared to reduced rainfall (−9%) using climate predictions for 2080. Fu et al.

(2022) also found that VPD triggered water stress and reduced carbon assimilation regardless of soil water deficits.

Our findings on the effect of increased VPD on simulated transpiration differed from other studies. Most studies have reported a net decline in cumulative transpiration as a result of increased VPD during seasonally dry periods (Eamus et al., 2013; Fang et al., 2021; Ruehr et al., 2014), whereas we observed a net increase in cumulative transpiration in our modeling scenarios with elevated VPD. For example, Ruehr et al. (2014) modeled a 9% decrease in growing season transpiration in response to a 4.5 °C increase in summer air temperature (40% increase in VPD). In contrast, we observed a 3% increase in cumulative transpiration under the same percentage increase in maximum daily VPD (~ +1.0 kPa in absolute terms). Although we found an increase in cumulative transpiration over the summer, we observed decreased daily transpiration rates when leaf water potential was low enough to increase water stress and restrict gas exchange (Fig. 6b). Daily transpiration rates only increased for elevated VPD scenarios if conditions were favorable for gas exchange (e.g., increase in daily maximum VPD did not substantially lower the leaf water potential). This suggests that the observed differences in transpiration between our study and Ruehr et al. (2014) may be due to differences in stomatal regulation between Douglas-fir and ponderosa pine trees, which are both isohydric but differ in their water use strategies, including leaf hydraulic conductance and leaf water potential at stomatal closure (Johnson et al., 2009). The minimum leaf water potential for Douglas-fir was −2.8 MPa in our study and only −1.8 MPa for ponderosa pine in Ruehr et al. (2014). Thus, ponderosa pine, with a more conservative minimum leaf water potential, are likely to close their stomata earlier in the day to prevent hydraulic failure, explaining the decrease in summer transpiration in response to warming. Additionally, the location of their study, east of the Cascade Mountains, is historically warmer and drier than the west slope of the Cascades, generally exposing ponderosa pine to greater VPD.

Model scenarios of decreased rainfall created relatively small reductions in GPP compared to scenarios of increased VPD. While shallow soil water was depleted earlier in the season for low rainfall scenarios, deep roots compensated for lack of water in shallow layers, and without atmospheric water stress, we found relatively small declines in GPP with decreasing rainfall. Because most roots are concentrated in the upper meter of soil, reducing rainfall by 10 to 100% caused cumulative transpiration to decrease by 2 to 16% over the summer. Although plant-available water decreased substantially in shallow layers with decreased rainfall (Fig. 5a), we found weighted soil water potential was greater than −1.5 MPa throughout the summer (Fig. 6a). This suggested that soil water from 100 to 200 cm was available to deep roots. Thus, even after we removed all the rainfall from the model during spring and summer, the values of leaf water potential remained above the minimum sustainable leaf water potential (−2.8 MPa) for most of the summer. However, by the end of August, leaf water potential was approximately −2.5 MPa in all rainfall scenarios, which suggested water stress was high regardless of antecedent rainfall amounts.

The convergence of soil water potential by the end of summer is explained by the feedbacks between soil water content and transpiration—while soil water decreased earlier in the growing season for scenarios with low rainfall inputs, all scenarios converged on a common minimum soil water (~0.12 cm^3 cm^3) at 20 and 50 cm depth by late summer (Fig. 5a). Because rainfall totals during late summer are relatively low to begin with (e.g., 13 mm between July and August in our baseline scenario), model scenarios that decreased rainfall by up to 100% during this time did not have a large impact on the amount of water that infiltrated the soil. However, decreasing rainfall during May and June, which together received ~15 times more rainfall than July and August, (Fig. 4a) is likely to change year-to-year variability in the soil moisture availability heading into these drier months.

Vegetation sensitivity to rainfall reductions depends on how water is stored belowground. In our study, rooting depth extended to 2 m, which is the maximum rooting depth reported for Douglas-fir (McMinn, 1963). In addition, mean annual rainfall was much larger than root-zone water storage capacity so that soil water storage was easily replenished by winter rains. Dralle et al. (2020) suggested that vegetation growing in a Mediterranean climate would be more sensitive to rainfall patterns at the end of the wet season than to annual rainfall if root-zone water storage capacity was low relative to the mean annual rainfall. Storage capacity is certainly low relative to annual rainfall at our study site, and we did observe notable differences in transpiration in response to decreased rainfall during May and June; however, these differences diminished over the summer dry season. Our results suggest that another factor is important for transpiration late in the growing season, namely, the absolute capacity for soil moisture storage within the rooting zone.

Our model simulations showed that soil moisture contents were 0.3 m^3 m^{-3} at the beginning of the growing season and declined to ~0.12 m^3 m^{-3} at the end of the growing season. This suggests that there were 36 cm of plant-available water present in the rooting zone at the beginning of the growing season, sufficient for 72 days at maximum simulated rates of transpiration (5 mm day^{-1}) and 163 days at the average transpiration rates simulated over the growing season (2.2 mm day^{-1}). Compare that to a hypothetical Douglas-fir stand growing in a 50-cm deep soil over impermeable bedrock where there would only be 9 cm of plant-available water at the beginning of the growing season, which would supply 41 days of water at 2.2 mm day^{-1}. The importance of summer precipitation in these two cases would be very different even though storage capacity in the rooting zone is much smaller than mean annual rainfall in both cases. Given that the severity of rainfall-induced drought depends on root-zone water storage capacity, additional analysis is needed to understand soil drought across a range of soil depths and subsurface properties in the Pacific Northwest region (McDonnell et al., 2018). However, information on rooting depth and soil hydraulic properties is currently lacking especially in deep (>1 m) soils and saprolite.

4.2. *Interactive effects of increased VPD and decreased rainfall on GPP and transpiration*

Decreased rainfall during spring and summer did not interact with increased VPD to substantially reduce GPP in model scenarios. Eliminating all spring and summer rainfall reduced cumulative GPP by 33 g C for all VPD scenarios, including the baseline scenario. This change in GPP was relatively small compared to the change due to a 2.5 kPa increase in max daily VPD, which decreased cumulative GPP from the baseline by 200 g C. Unlike our study, Ruehr et al. (2014) found that precipitation drought exacerbates water stress when combined with increased temperature and VPD. It is likely that the increase in soil water stress during hot droughts was due to the exhaustion of soil water resources at their site, which had shallower maximum rooting depth (~1 m) compared to our site (~2 m). We hypothesize the effect of decreased rainfall on GPP was relatively minor in our study because trees had access to deep soil water which allowed soil water potential to remain above −1.5 MPa throughout the extremely dry summer. This deep water served to support transpiration during the summer regardless of when shallow soil water was depleted—e.g., earlier in the summer for low rainfall scenarios or later in the summer for high rainfall scenarios (Fig. 5a). In addition, we observed only modest decreases in soil water content at 20, 50, and 100 cm (Fig. 5b) when we increased VPD from the baseline scenario, which led to increased transpiration from moist soils (Fig. 6b).

While transpiration might increase with VPD up to a point, elevated soil water stress can eventually lead to a decline in transpiration rates (Breshears et al., 2013). Research from Wind River Experimental Forest provided evidence that warmer temperatures in the spring could lead to greater soil water loss early in the growing season, setting the stage for more extreme drought effects in the summer (Jiang et al., 2019). We did not simulate increased temperature and VPD in the spring, but we hypothesize that elevated temperatures and VPD during April and May

could increase transpiration rates and lead to the depletion of shallow soil water earlier in the growing season. This may have led to significantly more water stress by late summer in our low rainfall simulations.

4.3. Study limitations

We used a model to independently assess the influence of VPD and rainfall on cumulative growing season transpiration and GPP. It was necessary to simulate these responses within a modeling framework because VPD and rainfall tend to co-vary across many temporal scales. As such, we intentionally isolated VPD and rainfall in our model scenarios to separate their individual effects on transpiration and GPP. Even though there is strong correlation between VPD and rainfall, plants may not respond to changes in these variables similarly over time. For example, rainfall events during spring and summer may alleviate soil water stress for days to weeks. However, the influence of those same rain events on VPD may last only hours and, thus, VPD would be unlikely to have a persistent effect on GPP and transpiration. In contrast, heat waves can create VPD extremes that can have long-term consequences for plant physiological function (Teskey et al., 2015) with relatively minor impacts on soil water decline. Moreover, deep subsurface water storage appeared to be critical in sustaining Douglas-fir transpiration in late summer and has been found to alleviate tree water stress in other seasonally dry environments (Hahm et al., 2020; McCormick et al., 2021). Thus, the impact of extreme VPD on plant function could become increasingly decoupled from the impact of seasonal rainfall deficits where trees have access to deep water storage. While forest water stress is likely to result from a combination of elevated VPD and reduced rainfall, in reality, we recommend future work prioritize monitoring and forecasting how deep-water storage may buffer forest drought stress and how VPD extremes may impact long-term forest health.

Future work is also needed to examine how our findings vary spatially especially in locations where observations of historic sap flow and ecosystem fluxes can be leveraged. For example, future simulations that include heterogeneity in vegetation and soil properties as well as microclimatic conditions across steep, varying terrain may improve predictions of carbon and water fluxes in mountainous landscapes. Additionally, the SPA model does not include macropore drainage due to coarse material such as rocks and roots which can have significant effects on soil water drainage during the wet season and thus the amount of soil moisture available to vegetation at the beginning of the summer dry season (Jarecke et al., 2021; Naseri et al., 2019). As a result, simulated SWC at 50 cm was overestimated especially during relatively wet periods in the spring and early summer (Fig. 2a). It is likely that soil water below one meter was also overestimated. Our simulations also assumed soil hydraulic properties did not change with depth over the 2 m profile. This simplification of soil hydraulic properties limited our capacity to evaluate the contribution of depth-dependent changes in soil water content on transpiration and GPP during the summer.

There is still much discussion about how to represent hydraulic constraints on stomatal behavior in ecosystem models, which control how the plant responds to drought stress (Wang et al., 2020). The SPA model uses an optimization approach that assumes plants balance carbon gain against hydraulic risk. However, the hydraulic risk is represented simply as a threshold value of leaf water potential, and stomatal conductance does not increase once this threshold is reached to avoid cavitation. In other models, more sophisticated hydraulic constraint functions, based on measurements of hydraulic vulnerability to cavitation of individual xylem elements, have been developed and implemented (Sperry et al., 2017; Venturas et al., 2018). While more mechanistic representation of hydraulic function and stomatal constraints may change the absolute simulated drought response, we do not expect the model improvement would alter our general conclusions.

5. Conclusion

The western slopes of the Cascades Mountains are projected to experience warmer temperatures during the summer and greater declines in spring and summer rainfall due to climate change. By disentangling the climatic controls on GPP and transpiration, we showed that decreased spring and summer rainfall is likely to have a smaller effect on forest productivity relative to increased temperature and VPD. We showed that decreased rainfall had a significant impact on cumulative transpiration and soil water content above 1 m; however, the access to deep (>1 m) soil water late in the summer mitigated water stress. This lack of soil water limitation led to relatively modest changes in soil and leaf water potential with decreasing rainfall. This suggested that the consequences of reduced precipitation during the growing season may be minimal in this region but will depend on subsurface water availability, which is determined by soil hydraulic properties and soil and rooting depths.

We found that elevated VPD expected with climate change will likely reduce forest productivity regardless of soil moisture availability at our site. Despite the co-occurrence of soil and atmospheric drought in many cases, heat-driven increases in VPD can lead to tree physiological water stress without soil water limitation. Substantial knowledge gaps remain, however, especially regarding the effect of large VPD and temperature anomalies on physiological function. In the future, field and modeling studies of Douglas-fir response to a warmer climate under varying conditions of subsurface water availability should be combined to provide greater insights into the mechanisms of forest response to climate change.

Declaration of Competing Interest

The authors declare that they have no known competing financial interests or personal relationships that could have appeared to influence the work reported in this paper.

Data availability

Data will be made available on request.

Acknowledgments

We thank the HJ Andrews staff for their support with project logistics and Zach Hoylman and Rob Livesay for assisting with field campaigns to install sensors and data loggers. Meteorological and sap flow observations were provided by the HJ Andrews Experimental Forest Long-Term Ecological Research Program (Daly et al., 2019; Moore and Bond, 2007). This research was funded by the National Science Foundation (LTER7 DEB 1440409), USDA Forest Service Pacific Northwest Research Station, and Oregon State University. LRH was supported by the National Science Foundation, Division of Environmental Biology, through the macrosystems biology and NEON-enabled science program grant number DEB-1802885. The use of trade or firm names in this publication is for reader information and does not imply endorsement by the U.S. Department of Agriculture of any product or service.

References

Bales, R.C., Goulden, M.L., Hunsaker, C.T., Conklin, M.H., Hartsough, P.C., O'Geen, A.T., Hopmans, J.W., Safeeq, M., 2018. Mechanisms controlling the impact of multi-year drought on mountain hydrology. Sci. Rep. 8, 1–8. https://doi.org/10.1038/s41598-017-19007-0.

Barnard, H.R., 2009. Inter-Relationships of Vegetation, Hydrology and Micro-Climate in a Young Douglas-fir Forest. Dissertation. Oregon State University.

Berner, L.T., Law, B.E., 2016. Plant traits, productivity, biomass and soil properties from forest sites in the Pacific Northwest, 1999-2014. Sci. Data 3, 1–14. https://doi.org/10.1038/sdata.2016.2.

Bonan, G.B., Williams, M., Fisher, R.A., Oleson, K.W., 2014. Modeling stomatal conductance in the earth system: linking leaf water-use efficiency and water transport along the soil-plant-atmosphere continuum. Geosci. Model Dev. 7, 2193–2222. https://doi.org/10.5194/gmd-7-2193-2014.

Bond, B.J., Kavanagh, K.L., 1999. Stomatal behavior of four woody species in relation to leaf-specific hydraulic conductance and threshold water potential. Tree Physiol. 19, 503–510. https://doi.org/10.1093/treephys/19.8.503.

Breshears, D.D., Adams, H.D., Eamus, D., Mcdowell, N.G., Law, D.J., Will, R.E., Williams, A.P., Zou, C.B., 2013. The critical amplifying role of increasing atmospheric moisture demand on tree mortality and associated regional die-off. Front. Plant Sci. 4, 2–5. https://doi.org/10.3389/fpls.2013.00266.

Brodribb, T.J., Powers, J., Cochard, H., Choat, B., 2020. Hanging by a thread? Forests and drought. Science 368, 261–266. https://doi.org/10.1126/science.aat7631.

Dalton, M.M., Mote, P.W., Snover, A.K., 2013. Climate Change in the Northwest. Implications for Our landscapes, Waters, and Communities. Island Press, Washington, DC.

Daly, C., Schulze, M., McKee, W., 2019. Meteorological data from benchmark stations at the HJ andrews experimental forest, 1957 to present. Long-Term Ecol. Res. https://doi.org/10.6073/pasta/c021a2ebf1f91adf0ba3b5e53189c84f.

Dralle, D.N., Jesse Hahm, W., Rempe, D.M., Karst, N., Anderegg, L.D.L., Thompson, S.E., Dawson, T.E., Dietrich, W.E., 2020. Plants as sensors: vegetation response to rainfall predicts root-zone water storage capacity in Mediterranean-type climates. Environ. Res. Lett. 15 https://doi.org/10.1088/1748-9326/abb10b.

Eamus, D., Boulain, N., Cleverly, J., Breshears, D.D., 2013. Global change-type drought-induced tree mortality: vapor pressure deficit is more important than temperature per se in causing decline in tree health. Ecol. Evol. 3, 2711–2729. https://doi.org/10.1002/ece3.664.

Fang, Y., Leung, L.R., Wolfe, B.T., Detto, M., Knox, R.G., McDowell, N.G., Grossiord, C., Xu, C., Christoffersen, B.O., Gentine, P., Koven, C.D., Chambers, J.Q., 2021. Disentangling the effects of vapor pressure deficit and soil water availability on canopy conductance in a seasonal tropical forest during the 2015 El Niño drought. J. Geophys. Res. Atmos. 126, 1–20. https://doi.org/10.1029/2021JD035004.

Farquhar, G.D., von Caemmerer, S., 1982. Modelling of photosynthetic response to the environment. Lange, O.L., Nobel, P.S., Osmond, C.B., Ziegler, H. Physiological Plant Ecology II. Encyclopedia of Plant Physiology, New Series. Springer-Verlag, Berlin, pp. 549–587.

Fu, Z., Ciais, P., Prentice, I.C., Bastos, A., Luo, X., Green, J.K., Gentine, P., Makowski, D., Stoy, P.C., Yang, H., Hajima, T., 2022. Atmospheric dryness reduces photosynthesis along a large range of soil water deficits. Nat. Commun. 1–10. https://doi.org/10.1038/s41467-022-28652-7.

Gabrielli, C.P., McDonnell, J.J., Jarvis, W.T., 2012. The role of bedrock groundwater in rainfall–runoff response at hillslope and catchment scales. J. Hydrol. 450 (451), 117–133. https://doi.org/10.1016/j.jhydrol.2012.05.023.

Grossiord, C., Buckley, T.N., Cernusak, L.A., Novick, K.A., Poulter, B., Siegwolf, R.T.W., Sperry, J.S., McDowell, N.G., 2020. Plant responses to rising vapor pressure deficit. New Phytol. https://doi.org/10.1111/nph.16485.

Grossiord, C., Sevanto, S., Borrego, I., Chan, A.M., Collins, A.D., Dickman, L.T., Hudson, P.J., McBranch, N., Michaletz, S.T., Pockman, W.T., Ryan, M., Vilagrosa, A., McDowell, N.G., 2017. Tree water dynamics in a drying and warming world. Plant Cell Environ. 40, 1861–1873. https://doi.org/10.1111/pce.12991.

Hahm, W.J., Dralle, D.N., Rempe, D.M., Bryk, A.B., Thompson, S.E., Dawson, T.E., Dietrich, W.E., 2019. Low subsurface water storage capacity relative to annual rainfall decouples Mediterranean plant productivity and water use from rainfall variability. Geophys. Res. Lett. 6544–6553. https://doi.org/10.1029/2019GL083294.

Hahm, W.J., Rempe, D.M., Dralle, D.N., Dawson, T.E., Dietrich, W.E., 2020. Oak transpiration drawn from the weathered bedrock vadose zone in the summer dry season. Water Resour. Res. 56, 1–24. https://doi.org/10.1029/2020WR027419.

Halpern, C.B., 1988. Early successional pathways and the resistance and resilience of forest communities. Ecol. Soc. Am. 69, 1703–1715.

Jarecke, K.M., Bladon, K.D., Wondzell, S.M., 2021. The influence of local and nonlocal factors on soil water content in a steep forested catchment. Water Resour. Res. 57, 1–21. https://doi.org/10.1029/2020wr028343.

Jiang, Y., Kim, J.B., Trugman, A.T., Kim, Y., Still, C.J., 2019. Linking tree physiological constraints with predictions of carbon and water fluxes at an old-growth coniferous forest. Ecosphere 10. https://doi.org/10.1002/ecs2.2692.

Johnson, D.M., Woodruff, D.R., McCulloh, K.A., Meinzer, F.C., 2009. Leaf hydraulic conductance, measured *in situ*, declines and recovers daily: leaf hydraulics, water potential and stomatal conductance in four temperate and three tropical tree species. Tree Physiol. 29, 879–887. https://doi.org/10.1093/treephys/tpp031.

Law, B.E., 2021. AmeriFlux BASE US-Me3 Metolius-second young aged pine, Ver. 4-5, AmeriFlux AMP. (Dataset). https://doi.org/10.17190/AMF/1246077.

Lawson, T., Blatt, M.R., 2014. Stomatal size, speed, and responsiveness impact on photosynthesis and water use efficiency. Plant Physiol. 164, 1556–1570. https://doi.org/10.1104/pp.114.237107.

Licata, J.A., 2003. Structural and Physiological Changes with Stand Age: Use of a Process-Based Model to Compare Carbon and Water Fluxes in Young and Old-Growth Douglas-fir /Western Hemlock Forest stands. Oregon State University. Thesis.

Littell, J.S., Peterson, D.L., Tjoelker, M., 2008. Douglas-fir growth in mountain ecosystems: water limits tree growth from stand to region. Ecol. Monogr. 78, 349–368. https://doi.org/10.1890/07-0712.1.

Liu, Y., Konings, A.G., Kennedy, D., Gentine, P., 2021. Global coordination in plant physiological and rooting strategies in response to water stress. Glob. Biogeochem. Cycles 35, 1–23. https://doi.org/10.1029/2020GB006758.

Marias, D.E., Meinzer, F.C., Woodruff, D.R., McCulloh, K.A., 2017. Thermotolerance and heat stress responses of Douglas-fir and ponderosa pine seedling populations from contrasting climates. Tree Physiol. 37, 301–315. https://doi.org/10.1093/treephys/tpw117.

Mauer, O., Palátová, E., 2012. Root system development in Douglas fir (Pseudotsuga menziesii [Mirb.] Franco) on fertile sites. J. For. Sci. 58, 400–409. https://doi.org/10.17221/94/2011-jfs.

McCormick, E.L., Dralle, D.N., Hahm, W.J., Tune, A.K., Schmidt, L.M., Chadwick, K.D., Rempe, D.M., 2021. Widespread woody plant use of water stored in bedrock. Nature 597, 225–229. https://doi.org/10.1038/s41586-021-03761-3.

McDonnell, J.J., Evaristo, J., Bladon, K.D., Buttle, J., Creed, I.F., Dymond, S.F., Grant, G., Iroume, A., Jackson, C.R., Jones, J.A., Maness, T., McGuire, K.J., Scott, D.F., Segura, C., Sidle, R.C., Tague, C., 2018. Water sustainability and watershed storage. Nat. Sustain. 1, 378–379. https://doi.org/10.1038/s41893-018-0099-8.

McKay, M.D., Beckman, R.J., Conover, W.J., 2000. A comparison of three methods for selecting values of input variables in the analysis of output from a computer code. Technometrics 42, 55–61. https://doi.org/10.1080/00401706.2000.10485979.

McMinn, R.G., 1963. Characteristics of Douglas-fir root systems. Can. J. Bot. 41, 105–122.

Meinzer, F.C., Johnson, D.M., Lachenbruch, B., McCulloh, K.A., Woodruff, D.R., 2009. Xylem hydraulic safety margins in woody plants: coordination of stomatal control of xylem tension with hydraulic capacitance. Funct. Ecol. 23, 922–930. https://doi.org/10.1111/j.1365-2435.2009.01577.x.

Monteith, J.L., Unsworth, M.H., 2008. Principles of Environmental Physics, 3rd ed. Elsevier, Amsterdam; Boston.

Moore, G.W., Adkison, C., Aparecido, L.M.T., Basant, S., Cooper, C.E., Cross, A.J., Deshpande, A., Catalan, M., Wright, C., 2020. Thermal dissipation sensors enter a new age: navigating frontiers in transpiration and hydrologic function. Acta Hortic. 1300, 37–46. https://doi.org/10.17660/ActaHortic.2020.1300.6.

Moore, G.W., Bond, B.J., 2007. Sap flow measurements to estimate overstory water use in Watersheds 1 and 2. Andrews Exp. For. 1999–2002.

Moore, G.W., Bond, B.J., Jones, J.A., Phillips, N., Meinzer, F.C., 2004. Structural and compositional controls on transpiration in 40-and 450-year-old riparian forests in western Oregon, USA. Tree Physiol. 24, 481–491. https://doi.org/10.1093/treephys/24.5.481.

Mote, P.W., Bethel, J., Capalbo, S.M., Dalton, M.M., Eigenbrode, S.E., Glick, P., Houston, L., Littell, J.S., Lynn, K., Raymondi, R.R., Reeder, W.S., Snover, A.K., 2013. Climate change in the northwest. Brief Summ. https://doi.org/10.5822/978-1-61091-512-0.

Naseri, M., Iden, S.C., Richter, N., Durner, W., 2019. Influence of stone content on soil hydraulic properties: experimental investigation and test of existing model concepts. Vadose Zo. J. 18 https://doi.org/10.2136/vzj2018.08.0163.

Novick, K.A., Ficklin, D.L., Stoy, P.C., Williams, C.A., Bohrer, G., Oishi, A.C., Papuga, S. A., Blanken, P.D., Noormets, A., Sulman, B.N., Scott, R.L., Wang, L., Phillips, R.P., 2016. The increasing importance of atmospheric demand for ecosystem water and carbon fluxes. Nat. Clim. Change 6, 1023–1027. https://doi.org/10.1038/nclimate3114.

Phillips, N., Bond, B.J., McDowell, N.G., Ryan, M.G., 2002. Canopy and hydraulic conductance in young, mature and old Douglas-fir trees. Tree Physiol. 22, 205–211. https://doi.org/10.1093/treephys/22.2-3.205.

Core Team R., 2021. R: a language and environment for statistical computing.

Restaino, C.M., Peterson, D.L., Littell, J., 2016. Increased water deficit decreases Douglas fir growth throughout western US forests. Proc. Natl. Acad. Sci. U. S. A. 113, 9557–9562. https://doi.org/10.1073/pnas.1602384113.

Ruehr, N.K., Law, B.E., Quandt, D., Williams, M., 2014. Effects of heat and drought on carbon and water dynamics in a regenerating semi-arid pine forest: a combined experimental and modeling approach. Biogeosciences 11, 4139–4156. https://doi.org/10.5194/bg-11-4139-2014.

Rupp, D.E., Li, S., Mote, P.W., Shell, K.M., Massey, N., Sparrow, S.N., Wallom, D.C.H., Allen, M.R., 2017. Seasonal spatial patterns of projected anthropogenic warming in complex terrain : a modeling study of the western US. Clim. Dyn. 48, 2191–2213. https://doi.org/10.1007/s00382-016-3200-x.

Saxton, K.E., Rawls, W.J., Romberger, J.S., Papendick, R.I., 1986. Estimating generalized soil water characteristics from texture. Soil Sci. Soc. Am. J. 5, 1031–1036.

Sperry, J.S., Venturas, M.D., Anderegg, W.R.L., Mencuccini, M., Mackay, D.S., Wang, Y., Love, D.M., 2017. Predicting stomatal responses to the environment from the optimization of photosynthetic gain and hydraulic cost. Plant Cell Environ. 40, 816–830. https://doi.org/10.1111/pce.12852.

Sulman, B.N., Roman, D.T., Yi, K., Wang, L., Phillips, R.P., Novick, K.A., 2016. High atmospheric demand for water can limit forest carbon uptake and transpiration as severely as dry soil. Geophys. Res. Lett. 9686–9695. https://doi.org/10.1002/2016GL069416.Received.

Teskey, R., Wertin, T., Bauweraerts, I., Ameye, M., McGuire, M.A., Steppe, K., 2015. Responses of tree species to heat waves and extreme heat events. Plant Cell Environ. 38, 1699–1712. https://doi.org/10.1111/pce.12417.

Topp, G.C., Davis, J.L., Annan, A.P., 1980. Electromagnetic determination of soil water content: measurements in coaxial transmission lines. Water Resour. Res. 16, 574–582. https://doi.org/10.1029/WR016i003p00574.

Venturas, M.D., Sperry, J.S., Hacke, U.G., 2017. Plant xylem hydraulics: what we understand, current research, and future challenges. J. Integr. Plant Biol. 59, 356–389. https://doi.org/10.1111/jipb.12534.

Venturas, M.D., Sperry, J.S., Love, D.M., Frehner, E.H., Allred, M.G., Wang, Y., Anderegg, W.R.L., 2018. A stomatal control model based on optimization of carbon gain versus hydraulic risk predicts aspen sapling responses to drought. New Phytol. 220, 836–850. https://doi.org/10.1111/nph.15333.

Wang, Y., Sperry, J.S., Anderegg, W.R.L., Venturas, M.D., Trugman, A.T., 2020. A theoretical and empirical assessment of stomatal optimization modeling. New Phytol. 227, 311–325. https://doi.org/10.1111/nph.16572.

Warren, J.M., Meinzer, F.C., Brooks, J.R., Domec, J.C., 2005. Vertical stratification of soil water storage and release dynamics in Pacific Northwest coniferous forests. Agric. For. Meteorol. 130, 39–58. https://doi.org/10.1016/j.agrformet.2005.01.004.

Wickham, H., 2021. tidyr: tidy Messy Data.

Wickham, H., 2016. ggplot2: Elegant graphics For Data Analysis. Springer-Verlag, New York.

Wickham, H., François, R., Henry, L., Müller, K., 2021. dplyr: a grammar of data manipulation.

Wilke, C.O., 2020. cowplot: streamlined plot theme and plot annotations for "ggplot2.".

Williams, M., Law, B.E., Anthoni, P.M., Unsworth, M.H., 2001. Use of a simulation model and ecosystem flux data to examine carbon-water interactions in ponderosa pine. Tree Physiol. 21, 287–298. https://doi.org/10.1093/treephys/21.5.287.

Williams, M., Rastetter, E.B., Fernandes, D.N., Goulden, M.L., Wofsy, S.C., Shaver, G.R., Melillo, J.M., Munger, J.W., Fan, S.M., Nadelhoffer, K.J., 1996. Modelling the soil-plant-atmosphere continuum in a Quercus-acer stand at Harvard forest: the regulation of stomatal conductance by light, nitrogen and soil/plant hydraulic properties. Plant Cell Environ. 19, 911–927. https://doi.org/10.1111/j.1365-3040.1996.tb00456.x.

Winner, W.E., Thomas, S.C., Berry, J.A., Bond, B.J., Cooper, C.E., Hinckley, T.M., Ehleringer, J.R., Fessenden, J.E., Lamb, B., McCarthy, S., McDowell, N.G., Phillips, N., Williams, M., 2004. Canopy carbon gain and water use: analysis of old-growth conifers in the Pacific Northwest. Ecosystems 7, 482–497. https://doi.org/10.1007/s10021-004-0139-2.

Zweifel, R., Steppe, K., Sterck, F.J., 2007. Stomatal regulation by microclimate and tree water relations: interpreting ecophysiological field data with a hydraulic plant model. J. Exp. Bot. 58, 2113–2131. https://doi.org/10.1093/jxb/erm050.